

# Automatic generation of helicity amplitudes in Feynman-Diagram gauge

Kaoru Haigiwara,<sup>1,\*</sup> Junichi Kanzaki,<sup>1,†</sup> Olivier Mattelaer,<sup>2,‡</sup>

Kentarou Mawatari,<sup>3,4,§</sup> and Ya-Juan Zheng<sup>3,¶</sup>

<sup>1</sup>*KEK Theory Center and Sokendai, Tsukuba, Ibaraki 305-0801, Japan*

<sup>2</sup>*CP3, Université Catholique de Louvain,*

*Chemin du Cyclotron, B-1348 Louvain la Neuve, Belgium*

<sup>3</sup>*Faculty of Education, Iwate University, Morioka, Iwate 020-8550, Japan*

<sup>4</sup>*Graduate School of Arts and Sciences,*

*Graduate School of Science and Engineering,*

*Iwate University, Morioka, Iwate 020-8550, Japan*

# Abstract

We develop a method to calculate helicity amplitudes of an arbitrary tree-level process in Feynman-Diagram (FD) gauge for an arbitrary gauge model with MadGraph5\_aMC@NLO. We start from the 't Hooft–Feynman gauge Lagrangian in FEYNRULES and generate scattering amplitudes by identifying the Goldstone boson as the 5<sup>th</sup> component of each weak boson. All the vertices of the 5-component weak bosons are then created automatically by assembling the relevant weak boson and Goldstone boson vertices in the Feynman gauge. The 5-component weak boson vertices are then connected by the  $5 \times 5$  matrix propagator in the FD gauge. As a demonstration of the method we calculate the cross section for the process  $\mu^- \mu^+ \rightarrow \nu_\mu \bar{\nu}_\mu t \bar{t} H$  with complex top Yukawa coupling, which can be obtained by adding a gauge invariant dimension-6 operator to the Standard Model (SM) Lagrangian. The FD gauge and the unitary (U) gauge amplitudes give exactly the same cross section, and subtle gauge theory cancellation among diagrams in the U gauge at high energies is absent in the FD gauge, as has been observed for various SM processes. In addition, we find that the total cross sections at high energies are dominated by a single, or a set of non-vanishing Feynman amplitudes with the higher dimensional vertices in the FD gauge.

## I. INTRODUCTION

Recently a new gauge boson propagator has been proposed for massless gauge bosons [1] and for massive gauge bosons [2, 3]. They can be obtained from the light cone (LC) gauge [3], where the gauge vector is chosen along the opposite of the gauge boson three momentum direction:

$$n(q)_{\text{FD}}^\mu = (\text{sgn}(q^0), -\vec{q}/|\vec{q}|). \quad (1)$$

This particular choice of the LC gauge vector has been named Feynman-Diagram (FD) gauge [2, 3], because of the common feature that subtle cancellation among interfering

---

\*Electronic address: kaoru.hagiwara@kek.jp

†Electronic address: kanzaki@post.kek.jp

‡Electronic address: olivier.mattelaer@uclouvain.be

§Electronic address: mawatari@iwate-u.ac.jp

¶Electronic address: yjzheng@iwate-u.ac.jp

Feynman diagrams is absent [1, 2], that the observable cross sections are dominated by a single Feynman diagram in the singular kinematical configuration where the Parton Shower description holds [1, 2, 4–6], and that some interference patterns away from the singular region seem to allow physical interpretation, such as the angular ordering of QCD radiations [3, 7, 8].

Because the subtle cancellation among interfering Feynman diagrams has been a severe obstruct in numerical evaluation of the amplitudes [9, 10], it is desirable that all numerical codes for the scattering amplitudes be available in the FD gauge. In QED and QCD, this is readily available since the only necessary change is to replace the photon and gluon propagators, which are given in the Feynman gauge in HELAS [11, 12] adopted by the series of MadGraph [13–16], one of the commonly-used matrix-element event generators. In the electroweak (EW) sector, we need to introduce new Feynman rules which treat the Goldstone bosons as the 5<sup>th</sup> component of the massive weak bosons.

In the paper [2], the  $5 \times 5$  FD gauge propagator of massive weak bosons [2, 5] has been derived from the unitary gauge propagator by making use of the BRST identities [17, 18], which relates the off-shell amplitudes of the scalar component of the weak boson  $\partial_\mu V^\mu$  and that of the corresponding Goldstone boson  $\pi_V$ . It has been found in ref. [2] that we need to introduce three new vertices,  $ZZZZ$ ,  $WWZH$  and  $WWAH$ , which do not appear in the Feynman rules of the Standard Model (SM) in the unitary gauge. In ref. [3], the FD gauge propagator has been obtained directly as the Green’s function of the equations of motion (EOM) of the LC gauge quantized EW theory. In this representation, it is clear that the Goldstone bosons are the 5<sup>th</sup> component of the weak boson, since the EOM mix all the five components.

In ref. [2], the FD gauge Feynman rules of the SM are obtained by supplying the above three 4-point vertices to the standard unitary gauge vertices, and then all the vertex functions among 5<sup>th</sup> components of the weak bosons have been coded manually. In ref. [3], the Feynman rules are obtained directly from the Lagrangian, since the Goldstone bosons are the 5<sup>th</sup> component of the massive weak bosons. Therefore, we already have the complete Feynman rules and the vertex function programs to calculate the tree-level scattering amplitudes in MadGraph5\_aMC@NLO (MG5AMC) [16] for an arbitrary process in the SM.

In this paper, we would like to extend the coverage to an arbitrary gauge model, where all the massive gauge bosons are obtained by the spontaneous breaking of gauge symmetries

in the scalar (Higgs) potential. We start from the FEYNRULES [19] model in the 't Hooft–Feynman gauge, and the Feynman rules and the corresponding vertex functions for numerical calculations of scattering amplitudes are automatically generated [20–22] in MG5AMC for an arbitrary gauge model. The key observation of ours is that all the gauge boson and the Goldstone boson vertices are gauge invariant, since the gauge dependence appears only in the propagators, i.e. in the weak boson and the Goldstone boson propagators in the covariant  $R_\xi$  gauge [23]. Therefore, all the vertex functions (the HELAS codes) generated in the Feynman gauge are valid also in the FD gauge. Our task is hence to combine them into the vertex function among the 5-component weak bosons, automatically. Once this is done, the  $5 \times 5$  weak boson propagators connecting two 5-component vertices should be the FD gauge propagators.

The paper is organized as follows: In section II, we explain how the weak boson and the Goldstone boson vertex functions (the HELAS codes) should be combined to make a new vertex function among the 5-component weak boson, automatically. In section III, we apply the method to a simplest extension of the SM, the SM effective field theory (SMEFT) [24–26] with a single dimension-6 operator. We select an operator which modifies the top quark Yukawa coupling to the Higgs boson, making it CP violating [27–32]. We show that the absence of subtle cancellation among interfering Feynman diagrams persists in the presence of non-Standard interactions. Section IV summarises our findings.

## II. FROM FEYNMAN GAUGE TO FEYNMAN-DIAGRAM GAUGE

In the original FD gauge papers [1–3], the amplitudes in the FD gauge have been calculated by using an independent HELAS library, which was coded manually and specifically prepared for all the SM vertices. However, in order to aid our pursuits for physics beyond the SM, it is necessary to automatically generate the codes to calculate FD gauge amplitudes for any processes in arbitrary gauge models. In this section, we show how this can be achieved in the framework of MG5AMC.

Since MG5AMC supports calculations in the Feynman gauge, it includes all the elements needed to incorporate calculations in the FD gauge. We, therefore, introduce a new command in MG5AMC in order to let the user change the gauge;

```
1 set gauge ***
```

where `***` can be `Feynman`, `unitary`, `axial` or `FD` for the FD gauge. Accordingly, we can now study any processes of interest in the FD gauge with only a few MG5AMC commands.<sup>1</sup> For instance, for the  $ZZ \rightarrow ZZ$  process:

```

1 MG5_aMC>import model sm
2 MG5_aMC>set gauge FD
3 MG5_aMC>generate z z > z z
4 MG5_aMC>output
5 MG5_aMC>launch

```

Without `"set gauge ***"`, MG5AMC employs the unitary gauge as a default gauge choice for massive gauge bosons. For the above process, there are three Higgs-exchanged diagrams in the unitary gauge. On the other hand, one additional four-point contact diagram exists in the FD gauge. We refer to Sec. 3.1 in ref. [2] for more details.

The command `"set gauge FD"` internally modifies both the representation of the model within MG5AMC and the way the ALOHA [22] code generates the HELAS subroutines. We describe each modification step-by-step below.

### (i) Extend vector boson wave functions from 4 components to 5 ones

Since the vector boson wave function (or polarization vector) for massive gauge bosons in the FD gauge includes the Goldstone boson component, the usual 4-component wave function  $\epsilon^\mu(p, \lambda)$  must be extended to the 5-component one  $\epsilon^M(p, \lambda)$ , where  $p$  and  $\lambda (= \pm 1, 0)$  are the momentum and the helicity of the vector boson, respectively, and the index  $M$  runs from 0 to 4,  $M = \{\mu, 4\}$ .

The HELAS vector boson wave function is a one-dimensional array of double complex numbers, with a four-momentum  $p^\mu$  defined in the first two slots of the wave function variable, `VC`:

```

1 (VC(1), VC(2)) = NSV (p(0) + i p(3), p(1) + i p(2))

```

An integer, `NSV`, is defined as `NSV=+1` if the vector boson is in the final state and `NSV=-1` if it is in the initial state.

---

<sup>1</sup> Note that the present FD gauge option in MG5AMC is restricted to LO/tree-level processes, both in standalone mode (evaluation of amplitude only) and in `madevent` mode (computation of cross-section and generation of unweighted events).

Normally, the following four complex numbers correspond to the vector boson wave function  $\epsilon^\mu(p, \lambda)$ :

```
1 (VC(3), VC(4), VC(5), VC(6))
```

This must be changed to the 5-component wave function  $\epsilon^M(p, \lambda)$  to include the Goldstone boson component as

```
1 (VC(3), VC(4), VC(5), VC(6), VC(7))
```

Appendix A.2 of ref. [2] includes the complete code for defining the vector boson wave function in the FD gauge.

## (ii) Identify Goldstone bosons as their associated gauge bosons

UFO models [20, 21] compatible with the Feynman gauge contain Goldstone bosons and their associated interactions. With the command `"set gauge FD"`, MG5AMC automatically, based on the mass, identify which Goldstone boson is associated with which vector boson, e.g.  $(\pi^\pm, \pi^0)$  as  $(W^\pm, Z)$  in the SM.

In each interaction vertex, all the Goldstone bosons are replaced by their associated vector bosons, while the color and Lorentz structures of the interaction are kept untouched.<sup>2</sup> If an interaction for the same particle content exists, the two interactions are merged into a single one.

For example, the interaction  $W^+\pi^-H$  present below in the UFO format:<sup>3</sup>

```
1 particles: [24, -251, 25], # W+ Pi- H
2 color: [c0 = 1 ],
3 lorentz: [VSS1 = P(1,2) - P(1,3)],
4 couplings: {(c0, VSS1): GC_37=-ee/(2.*sw)},
5 orders: {QED: 1},
```

will be merged with the interaction  $W^+W^-H$ :

```
1 particles: [-24, 24, 25], # W- W+ H
```

<sup>2</sup> This can lead to a warning due to the fact that a Lorentz structure for a scalar is attached to a spin-one particle.

<sup>3</sup> We do not exactly follow the UFO format to make it more readable/understandable for the reader.

```

2 color: [c0 = 1 ],
3 lorentz: [VVS1 = Metric(1,2)],
4 couplings: {(c0, VVS1): GC_72=(ee**2*complexi*vev)/(2.*sw**2)},
5 orders: {QED: 1},

```

One can note that the position of the  $W^+$  particle is not the same between the two interactions, and therefore, one needs to adapt the definition of the Lorentz (and, in principle, color) structure to the new ordering before actually doing the merge. The permutation of the indices is done automatically, and the new Lorentz and color structures are defined when/if needed (which, in this case, created the new SVS1 Lorentz structure). This procedure gives the following merge interaction:<sup>4</sup>

```

1 particles: [-24,24,25], # W- W+ H
2 color: [c0 = 1 ],
3 lorentz: [VVS1 = Metric(1,2),
4           SVS1 = P(2,1) - P(2,3)],
5 couplings: {(c0, VVS1): GC_72=(ee**2*complexi*vev)/(2.*sw**2),
6             (c0, SVS1): GC_37=-ee/(2.*sw)},
7 orders: {QED: 1},

```

One technical difficulty arises for interactions where, in the Feynman gauge, both the vector boson and its Goldstone boson counterpart are present. To make the issue clearer, we present an example for the case of the four-point interaction among two  $Z$  bosons and two of their Goldstone bosons in the SM:

```

1 particles: [23,23,250,250], # Z Z Pi0 Pi0
2 color: [c0 = 1 ],
3 lorentz: [VVSS1 = Metric(1,2)],
4 couplings: {(c0, VVSS1): GC_65=ee**2*i + (cw**2*ee**2*i)/(2*sw**2)
5             + (ee**2*i*sw**2)/(2*cw**2)},
6 orders: {QED: 2},

```

---

<sup>4</sup> Additional interactions like  $\pi^+W^-H$  will also be merged into the same interaction, but those are not shown here for clarity. We refer to Table 4 in ref. [2] for more details.

As described above, the interaction will be mapped into a new interaction with four  $Z$  bosons, which is not present neither in the Feynman gauge nor in the unitary gauge. The issue is that any pair of  $Z$  bosons need to be associated with a new Lorentz structure where they correspond to a Goldstone boson, leading to the final interaction containing six Lorentz structures. Five of those Lorentz structures are new and are generated automatically, given that they are identical to the original one up to the permutation of the indices. The new interaction is then given by:<sup>5</sup>

```

1 particles: [23,23,23,23], # Z Z Z Z
2 color: [c0 = 1 ],
3 lorentz: [VVSS1 = Metric(1,2) , VSVS1 = Metric(1,3) ,
4           VSSV1 = Metric(1,4) , SVVS1 = Metric(2,3) ,
5           SVSV1 = Metric(2,4) , SSVV1 = Metric(3,4)],
6 couplings: {(c0, VVSS1): GC_65, (c0, VSVS1): GC_65,
7             (c0, VSSV1): GC_65, (c0, SVVS1): GC_65,
8             (c0, SVSV1): GC_65, (c0, SSVV1): GC_65},
9 orders: {QED: 2},

```

### (iii) Multiply propagator factor

Each of the Lorentz structures of the new interactions will be passed to ALOHA to generate the standard HELAS subroutines. For the subroutines associated with a propagator for a gauge boson, we apply the following transformation to obtain the 5-component FD gauge current from the Feynman gauge current. Using the gauge vector in eq. (1) in the FD gauge, where  $q^\mu$  is the four-momentum of the propagating boson with the mass  $m$ , we convert the output current, `wf(0:3)` for the gauge boson and `wf(4)` for the associated Goldstone boson, to the current defined in the FD gauge, `wfd(0:4)`, as:

```

1 ci   = (0.d0,1.d0)
2 q(4) = -ci * m

```

<sup>5</sup> In the SM, a 7<sup>th</sup> Lorentz structure, not included here for clarity is associated with the  $ZZZZ$  interaction due to the presence in the Feynman gauge of another interaction with four Goldstone bosons. We refer to Table 5 in ref. [2] for more details.

```

3  nq      = n(0)*q(0) - n(1)*q(1) - n(2)*q(2) - n(3)*q(3)
4  js1     = (n(0)*wf(0) - n(1)*wf(1) - n(2)*wf(2) - n(3)*wf(3)) / nq
5  js2     = (q(0)*wf(0) - q(1)*wf(1) - q(2)*wf(2) - q(3)*wf(3)
6  &       - dconjg(q(4))*wf(4)) / nq
7  wfd(0:4) = wf(0:4) - q(0:4)*js1 - n(0:4)*js2

```

Here, the four vector,  $n^\mu$  in eq. (1), is expanded to  $n^M$  with  $n^4 = 0$ . See Sec. 2.2 as well as Appendix A in ref. [2] for details.

### III. AN EXAMPLE IN SMEFT

As a demonstration and a test of the above procedure, we apply the method in SMEFT with a dimension-6 operator [27–32]

$$\mathcal{L} = \mathcal{L}_{\text{SM}} + \left\{ \frac{C}{\Lambda^2} Q_3^\dagger t_R \tilde{\phi} \left( \tilde{\phi}^\dagger \tilde{\phi} - \frac{v^2}{2} \right) + \text{h.c.} \right\}, \quad (2)$$

where  $Q_3 = (t_L, b_L)^T$  and<sup>6</sup>

$$\tilde{\phi} = \left( \frac{v + H - i\pi^0}{\sqrt{2}}, -i\pi^- \right). \quad (3)$$

When we take the coefficient as [31]

$$\frac{C}{\Lambda^2} = \frac{\sqrt{2}(g_{\text{SM}} - g e^{i\xi})}{v^2}, \quad (4)$$

the phenomenological Lagrangian

$$\mathcal{L}_{tH} = -g\bar{t}(\cos \xi + i \sin \xi \gamma_5) t H, \quad (5)$$

for CP violating top quark Yukawa coupling is obtained. Throughout this section, we take

$$g = g_{\text{SM}} = \frac{m_t}{v}, \quad (6)$$

so that the only non-SM parameter is the CP phase,  $\xi$ . In the following,  $\xi = 0$  stands for the SM.

<sup>6</sup> We adopt the FEYNRULES notation for the Higgs doublet with hypercharge 1/2 which differs from the Higgs Lagrangian given in ref. [2] by the overall sign of the three Goldstone bosons.

By using the method described in section II, we generate the amplitudes for the process

$$\mu^- \mu^+ \rightarrow \nu_\mu \bar{\nu}_\mu t \bar{t} H, \quad (7)$$

in the tree-level by using MG5AMC. We find 118 Feynman diagrams in the FD gauge, compared to 89 diagrams in the unitary (U) gauge. The number of diagrams reduce to 89 in the FD gauge and 87 in the U gauge, respectively, in the SM. In order to study the interference patterns among the Feynman diagrams, we classify the diagrams into the following 6 subgroups:

$$\text{WWF} : W^- W^+ \text{ fusion}, \quad (8a)$$

$$\mu^- W^+ : \mu^- W^+ \text{ fusion}, \quad (8b)$$

$$W^- \mu^+ : W^- \mu^+ \text{ fusion}, \quad (8c)$$

$$\text{anni-}Z : \mu^- \mu^+ \text{ annihilation with } s\text{-channel } Z \text{ exchange}, \quad (8d)$$

$$\text{anni-}\gamma : \mu^- \mu^+ \text{ annihilation with } s\text{-channel } \gamma \text{ exchange}, \quad (8e)$$

$$\text{anni-}\mu : \mu^- \mu^+ \text{ annihilation with } t\text{-channel } \mu \text{ exchange}, \quad (8f)$$

which are illustrated in Fig. 1.

In short, the WWF diagrams (a) have two  $t$ -channel  $W$  propagators, one from the  $\mu^- \rightarrow \nu_\mu$  leg, the other from the  $\mu^+ \rightarrow \bar{\nu}_\mu$  leg. The  $\mu^- W^+$  diagrams (b) have one  $t$ -channel  $W$  propagator emitted from the  $\mu^+ \rightarrow \bar{\nu}_\mu$  leg, whereas the  $W^- \mu^+$  diagrams (c) have one  $t$ -channel  $W$  propagator emitted from the  $\mu^- \rightarrow \nu_\mu$  leg. The anni- $Z$  (d) and anni- $\gamma$  (e) diagrams have  $s$ -channel  $Z$  and  $\gamma$  exchange, respectively, while the anni- $\mu$  (f) diagrams contain  $t$ -channel  $\mu$  exchange.

In Table I, we summarize the numbers of Feynman diagrams given by MG5AMC for each group. The left column is for the SM, whereas the right column is for the SMEFT Lagrangian of eq. (2). In each column, the left-hand-side gives the diagram numbers in the U gauge, whereas the right-hand-side is for the FD gauge. In Fig. 2, we show the total cross section of the process eq.(7) as a function of the total colliding energy  $\sqrt{s}$  in the range  $0.5 \text{ TeV} < \sqrt{s} < 100 \text{ TeV}$  in the SM ( $\xi = 0$ ). For simplicity, we assume unpolarized muon beams. The left panel, Fig. 2(a) is for the U gauge, whereas the right panel, Fig. 2(b) is for the FD gauge. The total cross section, given by the black solid curves are identical between the two panels, showing the gauge invariance of the total sum of all the Feynman amplitudes,

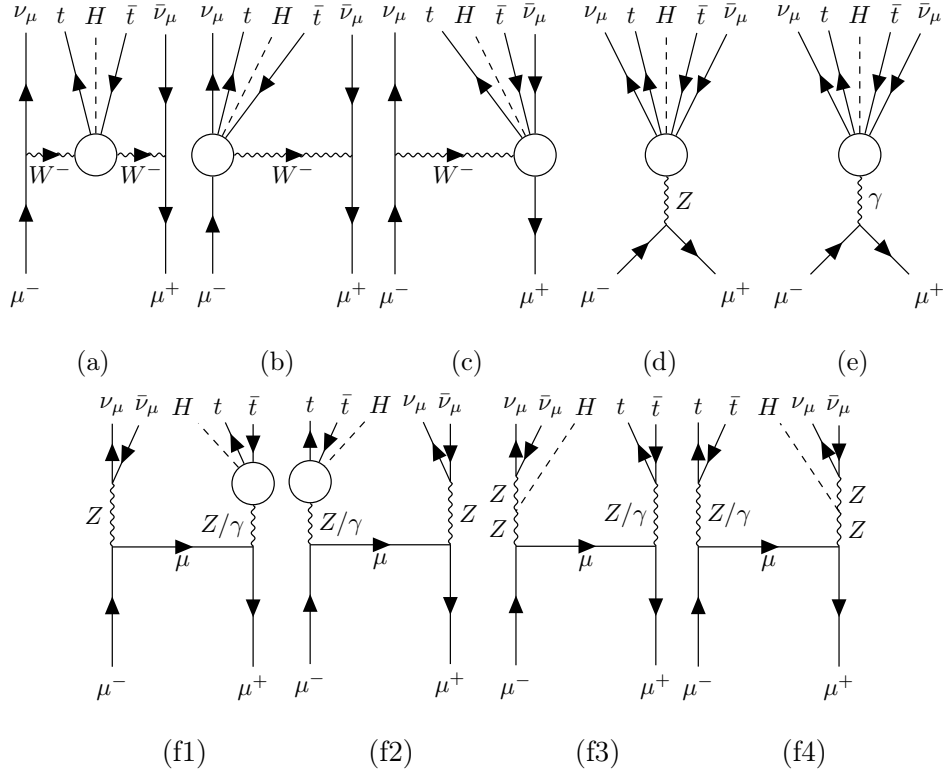


FIG. 1: The Feynman diagrams for the process  $\mu^- \mu^+ \rightarrow \nu_\mu \bar{\nu}_\mu t \bar{t} H$  are classified into six groups. (a) WWF:  $W^- W^+$  fusion; (b)  $\mu^- W^+$ :  $\mu^- W^+$  fusion; (c)  $W^- \mu^+$ :  $W^- \mu^+$  fusion; (d) anni- $Z$ :  $\mu^- \mu^+$  annihilation with  $s$ -channel  $Z$  exchange; (e) anni- $\gamma$ :  $\mu^- \mu^+$  annihilation with  $s$ -channel  $\gamma$  exchange; (f1-f4) anni- $\mu$ :  $\mu^- \mu^+$  annihilation with  $t$ -channel  $\mu$  exchange.

$\sum_k^{\text{all}} \mathcal{M}_k$ , and hence their absolute value square,

$$\left| \sum_k^{\text{all}} \mathcal{M}_k \right|^2, \quad (9)$$

which gives the observable cross section

$$\sigma = \frac{1}{2s} \frac{1}{2} \frac{1}{2} \sum_{\text{helicities}} \int \left| \sum_k^{\text{all}} \mathcal{M}_k \right|^2 d\Phi_{\nu_\mu \bar{\nu}_\mu t \bar{t} H}, \quad (10)$$

for unpolarized  $\mu$  beams, where  $\Phi_{\nu_\mu \bar{\nu}_\mu t \bar{t} H}$  stands for the final states phase space. Shown by the red solid curves are the total sum of the absolute square of each diagram, which is obtained by replacing the term (9) by

$$\sum_k^{\text{all}} |\mathcal{M}_k|^2, \quad (11)$$

No. of diagrams	SM		SMEFT	
	U	FD	U	FD
a) WWF	19	21	20	30
b) $\mu^- W^+$	11	11	11	13
c) $W^- \mu^+$	11	11	11	13
d) anni- $Z$	24	24	25	36
e) anni- $\gamma$	8	8	8	10
f) anni- $\mu$	14	14	14	16
<b>Total</b>	87	89	89	118

TABLE I: The number of Feynman diagrams given by MG5AMC for the process  $\mu^- \mu^+ \rightarrow \nu_\mu \bar{\nu}_\mu t \bar{t} H$ , with the six types of diagrams. The four columns give, from left to right, the SM in the U gauge, the SM in the FD gauge, the SMEFT model of eq. (2) in the U gauge, and in the FD gauge. The numbers represent the number of diagrams in each category.

in the cross section formula (10). Both in eqs. (9) and (11),  $\mathcal{M}_k$  stands for the amplitude of the diagram  $k$ , which runs from  $k = 1$  to 87 in the U gauge, from  $k = 1$  to 89 in the FD gauge in the SM, as given in the left bottom row of Table I. Helicity sum and average, as well as the phase space integrals are done exactly as for the total cross section.

The ratio of the red solid curve (11) obtained from the sum of the squared amplitudes and the total cross section given by the black solid curve obtained from the square of the total sum of the amplitudes (9)

$$R = \frac{\sum_{\text{helicities}} \int d\Phi \sum_k |\mathcal{M}_k|^2}{\sum_{\text{helicities}} \int d\Phi \left| \sum_k \mathcal{M}_k \right|^2}, \quad (12)$$

is a measure of subtle cancellation among interfering amplitudes. As is well known, the red solid curve grows rapidly with energy in the U gauge, making the ratio  $R$  from 92 at 1 TeV to  $1.8 \times 10^6$  and  $6.3 \times 10^9$  at 10 and 100 TeV, respectively. In the FD gauge, in contrast, the red solid curve has the same order of magnitude with the total cross section given by the black solid curve. The rate  $R$  is found to be 0.37, 2.8 and 4.9 at  $\sqrt{s} = 1, 10$  and 100 TeV, respectively.  $R > 1$  at  $\sqrt{s} \gtrsim 2$  TeV tells destructive interference among amplitudes.

Also shown in Fig. 2 are the partial contribution of the subsets of diagrams identified in

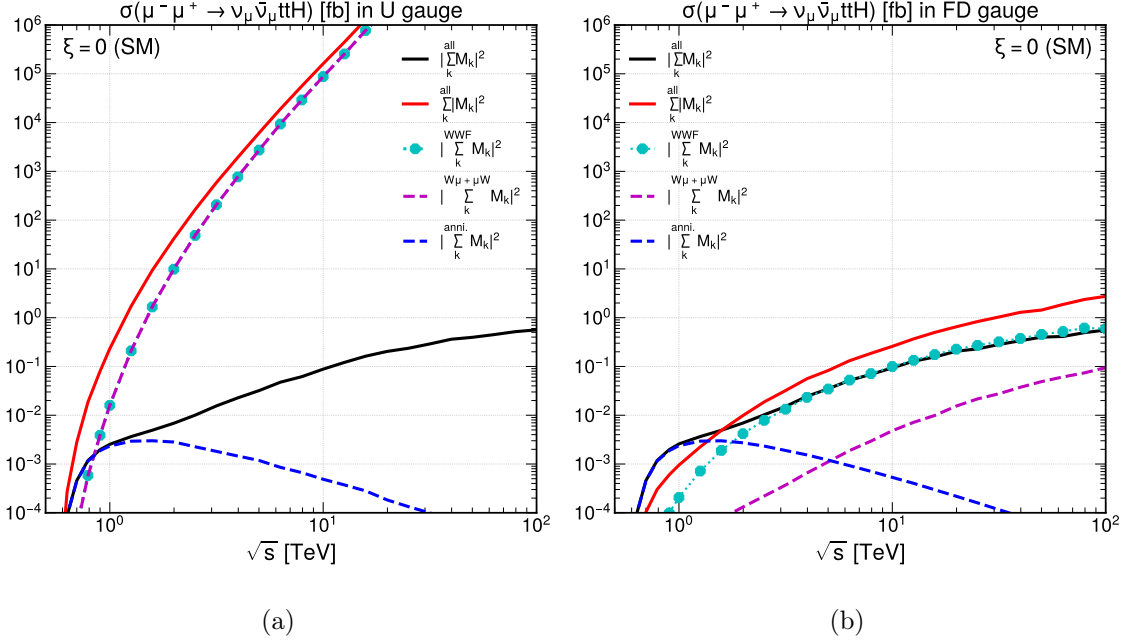


FIG. 2: Total cross section of  $\mu^- \mu^+ \rightarrow \nu_\mu \bar{\nu}_\mu t\bar{t}H$  at  $\xi = 0$  (SM). The black-solid line denotes the total cross section  $|\sum_k^{\text{all}} \mathcal{M}_k|^2$  with 87 diagrams in the U gauge (a) and with the 89 diagrams in the FD gauge (b). The red solid curve denoted as  $\sum_k^{\text{all}} |\mathcal{M}_k|^2$  gives the contribution of the total sum of the squares of each diagram. The cyan dotted line with circle denoted as  $|\sum_k^{\text{WWF}} \mathcal{M}_k|^2$  gives the contribution of  $W$  boson fusion diagrams. The magenta dashed line denoted as  $|\sum_k^{W\mu+\mu W} \mathcal{M}_k|^2$ , gives the contribution of all single  $W$  exchange diagrams. The blue dotted line denoted as  $|\sum_k^{\text{anni.}} \mathcal{M}_k|^2$  gives the contribution of all the annihilation type diagrams.

eq. (8) and in Fig. 1, while the number of diagrams in each subset is given in Table I. The cyan dotted lines with solid circle show the contribution of all the diagrams in the WWF category subgroup (a);

$$|\sum_k^{\text{WWF}} \mathcal{M}_k|^2, \quad (13)$$

the magenta dashed curves stand for the contribution of single  $W$  exchange diagrams of the groups (b) and (c);

$$|\sum_k^{W\mu+\mu W} \mathcal{M}_k|^2, \quad (14)$$

and finally the blue dashed curves give the total contribution of all the annihilation diagrams

$k$  in the groups (d), (e) and (f);

$$|\sum_k^{\text{anni.}} \mathcal{M}_k|^2. \quad (15)$$

We first note that the blue dashed curves are identical between the U and FD gauges, because the total sum of (d), (e) and (f) diagrams are identical to the full amplitudes for the processes,

$$\mu^- \mu^+ \rightarrow \nu_e \bar{\nu}_e t \bar{t} H, \quad (16)$$

(or  $\mu^- \mu^+ \rightarrow \nu_\tau \bar{\nu}_\tau t \bar{t} H$ ) provided that the model satisfies the  $\mu - e(\tau)$  universality. The breakdown of the annihilation amplitudes will be studied at the end of this section.

In the U gauge, Fig. 2(a), both the magenta and cyan curves are far larger than the total cross section, and that they are degenerate in the entire energy range. The two curves are about  $1.0 \times 10^6$  ( $4.4 \times 10^9$ ) times larger than the total cross section curve at  $\sqrt{s} = 10$  (100) TeV. These numbers are of the same order of magnitude of the ratio  $R$  as defined in eq. (12). This tells that the subtle cancellation takes place between the WWF type diagrams (a) and the single  $W$  exchange diagrams (b) and (c) in the U gauge.

In the FD gauge, shown in Fig. 2(b), in contrast, the cyan dotted curve for the WWF amplitudes saturates the total cross section at  $\sqrt{s} \gtrsim 3$  TeV. This agrees with the expectation that the 5-component weak boson representation gives the weak boson fusion amplitudes with the physical weak boson PDF, as pointed out first by Kunszt and Soper in the axial gauge [33]. It has been shown in ref. [3] that the FD gauge propagator of the weak bosons is identical to the axial gauge propagator of ref. [33] by taking the LC gauge limit. The single  $W$  exchange diagram contributions, depicted by the magenta dashed curve, are about a factor of 5 below the total cross section at the highest energy of  $\sqrt{s} \sim 100$  TeV. The absence of subtle cancellation, the saturation of the total cross section by the WWF type contributions, and the dominance of the annihilation contributions at low energies ( $\sqrt{s} \lesssim 1$  TeV) are all consistent with a physical picture based on the weak boson PDF approximation [10, 33, 34]. From Fig. 2(b), we can tell that the total cross section is slightly below the WWF contribution at highest energies ( $\sqrt{s} \gtrsim 50$  TeV), where the red and black solid curve ratio of  $R \sim 3.6$  suggests destructive interference among WWF and single  $W$  exchange amplitudes. Studying further details of the interference patterns among the FD gauge amplitudes is

beyond the scope of the present paper, whose aim is mainly to demonstrate the validity of the prescription given in section II.

In Figs. 3(a) and (b), we show the same set of curves in the presence of the non-SM phase,  $\xi = 0.1\pi$ . Both the black solid curve for the total cross section and the blue dashed curve for the annihilation contribution are identical between the U gauge (a) and the FD gauge (b), as expected. The total cross section (black solid curve) is not sensitive to the non-SM phase of  $|\xi| = 0.1\pi$  at low energies ( $\sqrt{s} \lesssim 1.2$  TeV), while it becomes about a factor of 3 times larger than the SM cross section at  $\sqrt{s} \sim 10$  TeV, about a factor of 20 times larger at  $\sqrt{s} \sim 100$  TeV. This has been observed first in ref. [31] in the U gauge, and our results in Fig. 3(b) confirms that we obtain the same results in the FD gauge, following the prescription given in section II.

Subtle gauge theory cancellation between the contribution of the  $W^-W^+$  fusion diagrams (cyan dotted curve dabbd WWF) and that of the single weak boson exchange diagrams (magenta dashed curve dabbd  $W^-\mu^+ + \mu^-W^+$ ) in the U gauge remains similar as in the SM case, shown in Fig. 2(a). This has been expected, since there is only one additional diagram in the U gauge for the  $W^-W^+$  fusion amplitudes, whose contribution has been evaluated in terms of the  $W_L^-W_L^+ \rightarrow t\bar{t}H$  amplitudes in ref. [31]. Therefore, subtle cancellation in the U

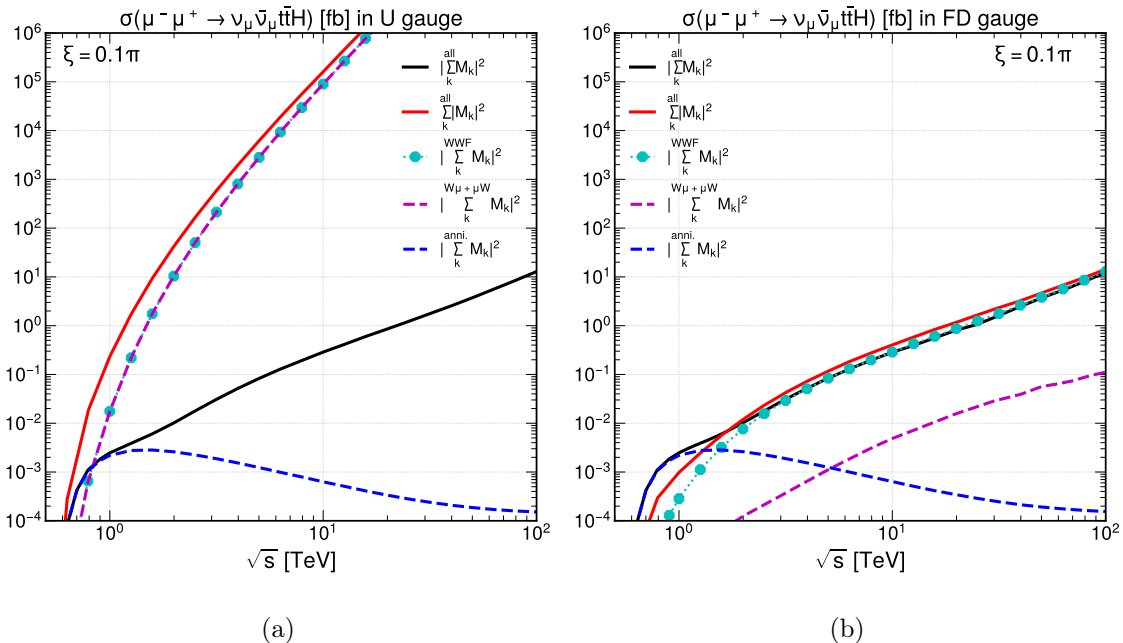


FIG. 3: Cross section of  $\mu^- \mu^+ \rightarrow \nu_\mu \bar{\nu}_\mu t \bar{t} H$  with  $\xi = 0.1\pi$ . The line types are the same as in Fig. 2.

gauge takes place between the WWF and single  $W$  exchange ( $W^- \mu^+ + \mu^- W^+$ ) diagrams, just as in the SM. In fact, we cannot observe significant  $\xi$  dependence in the three rapidly growing curves between Fig. 2(a) and Fig. 3(a). The  $\xi$  dependence of the total cross section, where the black solid curve in Fig. 3 grows more rapidly with the colliding energy  $\sqrt{s}$  than the SM prediction in Fig. 2, is obtained in the U gauge only after subtle cancellation among amplitudes of huge magnitude.

In a sharp contrast, we can make the following observation by comparing the  $\xi = 0.1\pi$  results in Fig. 3(b) and the  $\xi = 0$  (SM) results in Fig. 2(b) in the FD gauge: the total cross section is dominated by the WWF contribution at high energies, both in the SM and for  $\xi = 0.1\pi$ , and the rising total cross section at high energies for  $\xi = 0.1\pi$  is due to the rise of the WWF contribution. We do not observe significant  $\xi$  dependence in the single  $W$  exchange contribution ( $W^- \mu^+ + \mu^- W^+$ ), shown by the magenta dashed curve both in the Figs. 2(b) and 3(b).

In ref. [31], the high energy behavior of the total cross section has been calculated by assuming the dominance of the longitudinally polarized weak boson fusion subprocess,

$$W_L^- W_L^+ \rightarrow t \bar{t} H, \quad (17)$$

and then by approximating its cross section by that of the corresponding Goldstone collision process,

$$\pi^- \pi^+ \rightarrow t \bar{t} H. \quad (18)$$

The Goldstone boson equivalence theorem [35, 36] tells that the helicity amplitudes for the above two processes satisfy

$$\mathcal{M}(W_L^- W_L^+ \rightarrow t_h \bar{t}_{\bar{h}} H) = \mathcal{M}(\pi^- \pi^+ \rightarrow t_h \bar{t}_{\bar{h}} H) \left\{ 1 + \mathcal{O}\left(\frac{m_W^2}{E_W^2}\right) \right\}, \quad (19)$$

where  $h$  and  $\bar{h}$  are  $t$  and  $\bar{t}$  helicities, respectively. In particular, the high energy limit of the helicity amplitudes for the Goldstone boson collision process (18) have been calculated analytically [31] by using the dimension-6 vertex in the effective Lagrangian (2):

$$\mathcal{L}_{t\bar{t}H\pi\pi} = \frac{g_{\text{SM}} - g e^{i\xi}}{v^2} t_L^\dagger t_R H \pi^+ \pi^- + \text{h.c.} \quad (20)$$

The above term gives the only dimension-6 vertex which contributes to the process (18), and the corresponding amplitudes should dictate the high energy behavior. This has been

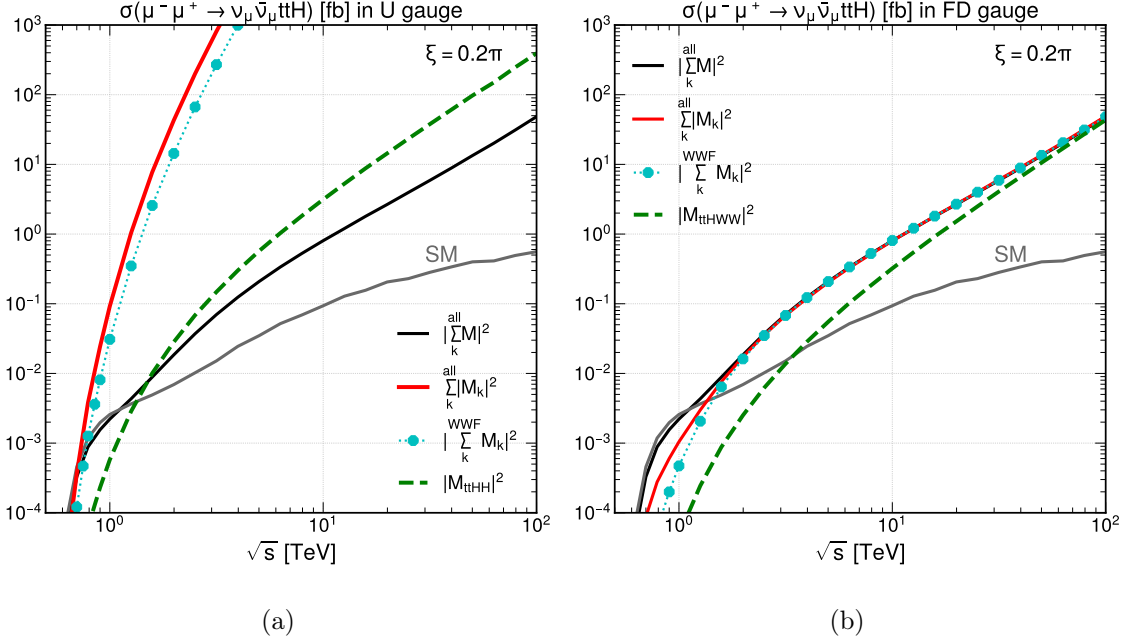


FIG. 4: Cross section of  $\mu^- \mu^+ \rightarrow \nu_\mu \bar{\nu}_\mu t \bar{t} H$  with  $\xi = 0.2\pi$  in the U gauge (a) and in the FD gauge (b). The black solid curve denotes the total cross section. The red solid curve gives the contribution of the total sum of the squares of each diagram. The cyan dotted curve gives the contribution of the  $W$  boson fusion diagrams. The green dashed curve shows the contribution of the single diagram with the contact  $ttHH$  vertex,  $\mathcal{M}_{ttHH}$  in the U gauge (a) and that of the diagram  $\mathcal{M}_{ttHWW}$  in the FD gauge (b) with the contact  $ttHWW$  vertex. The SM cross section ( $\xi = 0$ ) is given by the gray solid line as a reference.

confirmed in ref. [31] by comparing the analytic Goldstone boson amplitudes and the helicity amplitudes of the WWF subprocess (17) evaluated numerically by using MG5AMC in the U gauge.

In Fig. 4, we show the total cross section for the  $\mu^- \mu^+$  collision process (7) for  $\xi = 0.2\pi$  by the black solid curve. As a reference, the SM prediction ( $\xi = 0$ ) is given by the grey solid curve. In addition to the red solid curve for the sum of squares of each amplitude and the cyan dotted curve for the WWF contribution, in Fig. 4(b) we show by green dashed curve the contribution of the dimension-6 vertex (20) in the FD gauge,  $|\mathcal{M}_{ttHWW}|^2$ , depicted as the Feynman diagram Fig. 5(b). It is clearly seen from Fig. 4(b) that the total cross section is dominated by the WWF contribution at  $\sqrt{s} \gtrsim 3$  TeV, and then it is dominated by  $|\mathcal{M}_{ttHWW}|^2$  at  $\sqrt{s} \gtrsim 100$  TeV, in the FD gauge. This is an example of the property of the

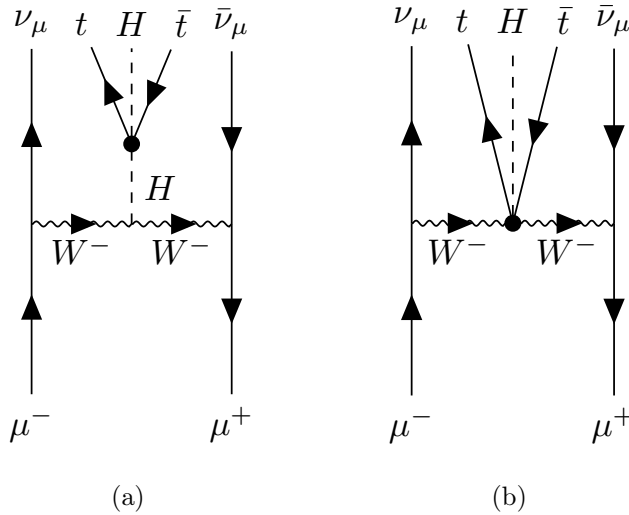


FIG. 5: Feynman diagram with the contact  $ttHH$  vertex (a) in both the U and FD gauges and the  $ttHWW$  vertex (b) in the FD gauge only.

FD gauge amplitudes, where the Goldstone boson equivalence is manifest [5, 6].

Shown in Fig. 4(a) are the results for the U gauge. As in Figs. 2(a) and 3(a), both the sum of squares of each amplitude (red solid) and the WWF contribution (cyan dotted) grow rapidly with energy, while the physical cross section (black solid) is exactly the same as the FD gauge. In the figure, we show by green dashed curve the contribution of the single Feynman diagram of Fig. 5(a), which has the  $ttHH$  vertex,

$$\mathcal{L}_{ttHH} = \frac{3(g_{\text{SM}} - ge^{i\xi})}{2v} t_L^\dagger t_R H^2 + \text{h.c.}, \quad (21)$$

whose mass dimension is 5. In the U gauge, the above  $ttHH$  vertex is the only interactions whose mass dimension is larger than 4. The green dashed curve grows with energy faster than the total cross section shown by the black solid curve, and is about a factor of 8 larger than the total cross section at  $\sqrt{s} \sim 100$  TeV. At this energy, the red solid curve gives  $3.9 \times 10^9$  fb, or about  $8.0 \times 10^7$  times larger than the total cross section. This again confirms the findings of ref. [31], where the amplitudes of the diagram Fig. 5(a), or its WWF subamplitudes have been evaluated analytically.

Summing up, the FD gauge amplitudes are free from subtle gauge cancellation among interfering diagrams, and the total cross section for the process (7) is dominated by the weak boson fusion (WWF) subamplitudes at high energies, both in the SM, and with nonzero CP phase  $\xi$ . The Goldstone boson equivalence between the longitudinally polarized weak boson

and its associated Goldstone boson is manifestly realized in the FD gauge amplitudes. In addition, we find that the high energy behavior of the FD gauge amplitudes are dictated by the amplitudes with the highest dimensional vertex.

In the rest of this section, we examine the annihilation amplitudes, whose contribution given by blue dashed curves in Figs. 2 and 3 are identical between the U gauge and the FD gauge. This simply reflects the fact that the ‘annihilation’ diagrams consist of a gauge invariant subset of the amplitudes, which corresponds to the full set of Feynman diagrams for a certain physical process such as the process in eq. (14), where the final neutrino flavor in the process (7) is changed from  $\nu_\mu$  to  $\nu_e$  (or  $\nu_\tau$ ). All the non-annihilation diagrams are then forbidden by the muon number conservation in the SM.

In Fig. 6, we show the total cross section of the process  $\mu^- \mu^+ \rightarrow \nu_e \bar{\nu}_e t \bar{t} H$ , eq. (16) as a function of the colliding muon pair energy, in the U gauge (a) and in the FD gauge (b). In addition to the total cross section given by the black solid line, we show the contributions of the three subgroups, those of the  $t$ -channel muon exchange diagrams in blue dashed curves, those of the  $s$ -channel  $\gamma$  exchange diagrams in magenta dashed curves, and the  $s$ -channel  $Z$  exchange diagrams by cyan dashed curves. We find that not only the total cross section given by the black solid curves, but also all the three subgroups of the amplitudes give exactly the same cross section in Figs. 6(a) and (b). Although there is no physical process in the SM which is given by the diagrams of the three annihilation subgroups, we can retain the  $s$ -channel  $\gamma$  or  $Z$  exchange diagrams only by changing the  $SU(2) \times U(1)$  quantum numbers of the muon. We can hence regard the subgroups of Feynman diagrams as the full set of diagrams for the annihilation of such exotic leptons.

The total sum of the squares of each Feynman amplitude is shown by red solid curves. We observe rapid growth of the red curve in the U gauge, as shown in Fig. 2(b) for the process (7). The ratio  $R$  of the red and black solid curves in Fig. 6(a), is about 60 at  $\sqrt{s} = 1$  TeV, which grows rapidly to about  $1.0 \times 10^8$  at  $\sqrt{s} = 10$  TeV, and  $5.9 \times 10^{13}$  at  $\sqrt{s} = 100$  TeV, which grows even faster with energy than what we find for the process (7) in Fig. 2(a).

In Fig. 6(b), we find that the red solid curve is consistently below the black solid curve for the total cross section, where the ratio  $R$  of eq. (12) is about 0.24, 0.60 and 0.79, at  $\sqrt{s} = 1, 10, \text{ and } 100$  TeV, respectively. The  $R$  value below unity tells an overall constructive interference among Feynman amplitudes. We find that the total cross section (black solid curve) is approximately the sum of the three subamplitude contributions.

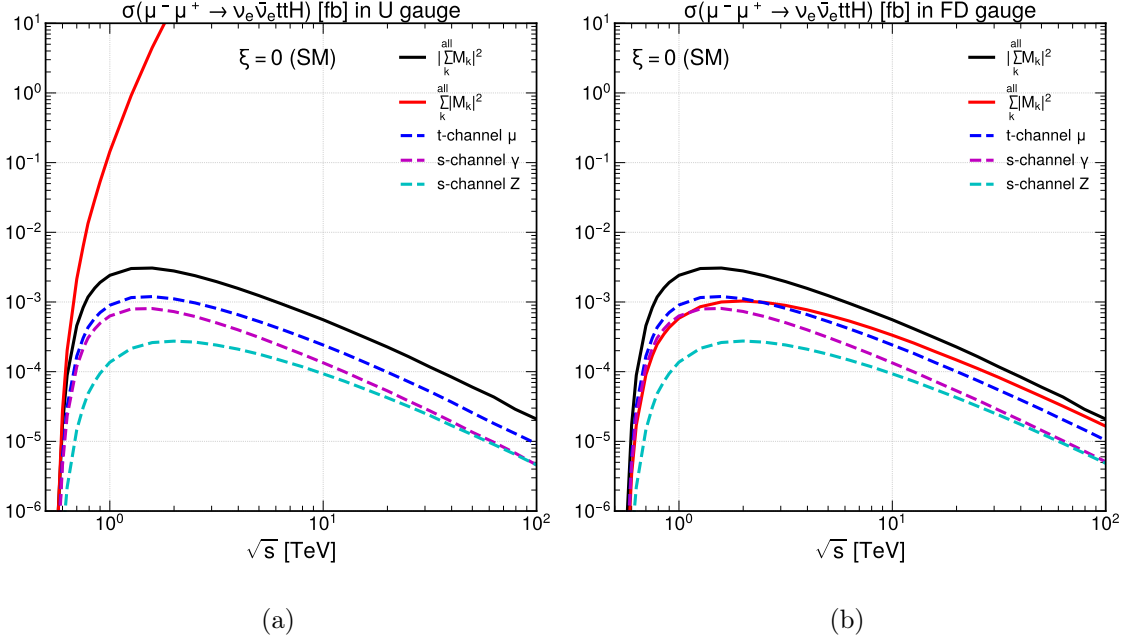


FIG. 6: Cross section of  $\mu^- \mu^+ \rightarrow \nu_e \bar{\nu}_e t \bar{t} H$  for  $\xi = 0$  (SM) for (a) U gauge, and (b) for FD gauge. The black solid line is the total cross section. The red solid line is for the  $\sum_k^{\text{all}} |\mathcal{M}_k|^2$ , summing up the squared of each amplitude. The blue dashed line is summing up the  $t$ -channel  $\mu$  exchange diagram. The magenta dashed line is summing up the photon exchange diagram. The cyan dashed line is summing up the  $s$ -channel  $Z$  exchange diagrams.

Finally, in Figs.7(a) and 7(b), we show the results for our effective Lagrangian model (2), when the CP phase value is  $\xi = 0.2\pi$ . The total cross section is given by the black solid curves, while we also show the SM ( $\xi = 0$ ) results from Fig.6 by grey solid curves, which are both exactly the same between in the U gauge (a) and the FD gauge (b). The ratio  $R$  of the red and black solid curves, eq. (12), grows rapidly with energy in the U gauge, from 77 at 1 TeV, to  $6.1 \times 10^7$  at 10 TeV and  $2.3 \times 10^{12}$  at 100 TeV, respectively. These values are similar to the SM case reported above for Fig.6(a), and hence the interference pattern in the U gauge is not affected significantly by the presence of the non-SM interactions in our effective Lagrangian model of eq. (2).

The  $\xi$  dependence of the total cross section has been reported systematically in ref. [31]. It can also be learned from comparing the black and grey solid curves, which are common between Figs.7(a) and (b). The total cross section for  $\xi = 0.2\pi$  is slightly smaller than the SM cross section at  $\xi = 0$  below  $\sqrt{s} \sim 3$  TeV, which confirms the trend observed in

refs. [37–43] for the process

$$e^-e^+ \rightarrow t\bar{t}H, \quad (22)$$

since the process (16) can be regarded as a  $Z$  boson emission correction to the process (22), and hence the  $\xi$  dependence should be similar at low energies. At high energies,  $\sqrt{s} \gtrsim 5$  TeV, the black curve stays above the grey curve for the SM cross section, and decreases very slowly with energy, reaching about  $5 \times 10^{-4}$  fb at 100 TeV. Because the total cross section decreases with energy in the SM, the cross section is about 1.7 and 26 larger than the SM at  $\sqrt{s} = 10$  and 100 TeV, respectively. The asymptotically constant behavior of the total cross section suggests contribution of higher dimensional interactions in the effective Lagrangian model (2). Shown in Fig. 8(a) is the Feynman diagram with the  $ttHH$  vertex, whose mass dimension is 5. In the U gauge, where all the Goldstone boson vertices are inactive, this is the only diagram with higher dimensional vertex. We show by green dashed curve the contribution of the diagram Fig. 8(a) in the U gauge, labeled as  $|\mathcal{M}_{ttHH}|^2$ . The single diagram

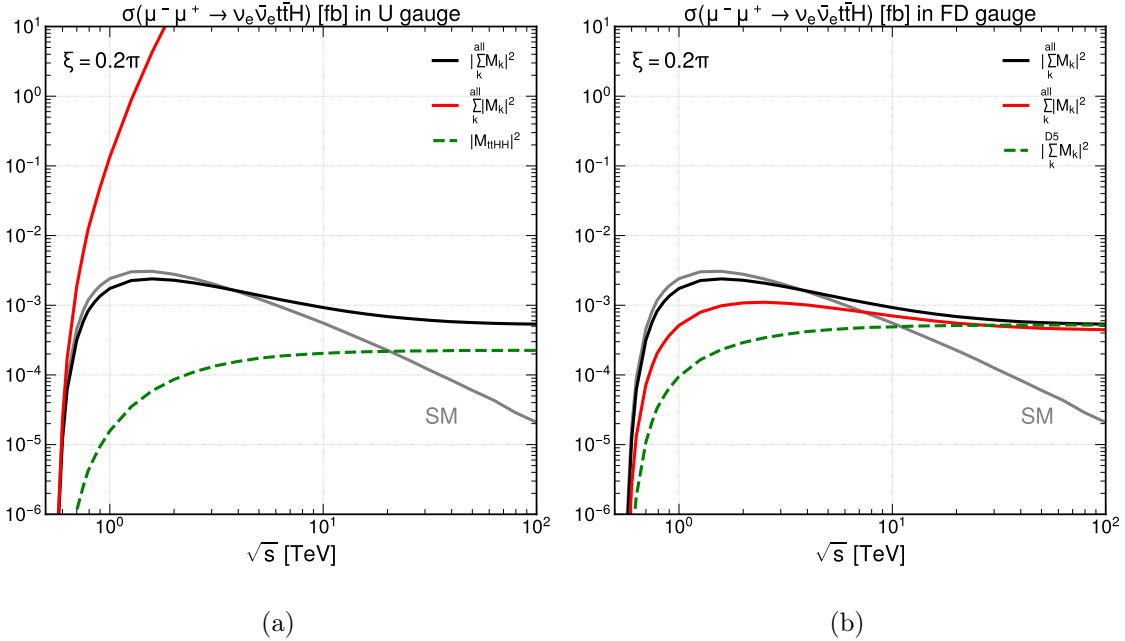


FIG. 7: Cross section of  $\mu^- \mu^+ \rightarrow \nu_e \bar{\nu}_e t \bar{t} H$  for the  $\xi = 0.2\pi$  in the U gauge (a), and in the FD gauge (b). The line types are the same as Fig. 4, where the green dashed curve shows the contribution of the diagram with the dimension-5  $ttHH$  vertex in the U gauge (a), while it shows the contribution of all the diagrams with dimension-5 vertices  $ttHH$ ,  $ttHZ$  and  $ttZZ$  in the FD gauge (b).

contribution given by the green curve grows with energy and has similar energy dependence with the black curve at highest energies, reaching about 40% of the total cross section at  $\sqrt{s} = 100$  TeV. The red solid curve for the total sum of squares of each amplitude grows rapidly with energy just as in Fig. 6(a) for the SM. Therefore, subtle gauge cancellation in the U gauge is not affected significantly by the presence of the non-SM interactions in the effective Lagrangian (2).

From Table I, we have 47 Feynman diagrams for the process (16) in the U gauge. One of these 47 diagrams is the one given by Fig. 8(a),  $\mathcal{M}_{ttHH}$ , and the remaining 46 diagrams don't contain higher dimensional vertices. The results shown in Fig. 7(a) for the U gauge tell us, e.g. at  $\sqrt{s} = 100$  TeV, the total sum of the 46 Feynman diagrams gives, after subtle gauge cancellation, the amplitudes whose magnitude is similar to  $|\mathcal{M}_{ttHH}|$ . Although the energy and the kinematical dependences of  $|\mathcal{M}_{ttHH}|^2$  can be understood from the analytic expression of the diagram Fig. 8(a), that the total sum of the remaining 46 amplitudes give similar amplitudes at high energies tells us a miraculous aspect of gauge cancellation in the U gauge.

In Fig. 8(b), we show the Feynman diagram with the  $ttHZZ$  vertex, which is the only dimension-6 vertex in the effective Lagrangian of eq. (2). Because the corresponding diagram with the dimension-6  $ttHWW$  vertex in Fig. 5(b) has been found to dominate the total cross section of the process (7) at high energies, as shown by green dashed curve in Fig. 4(b), we

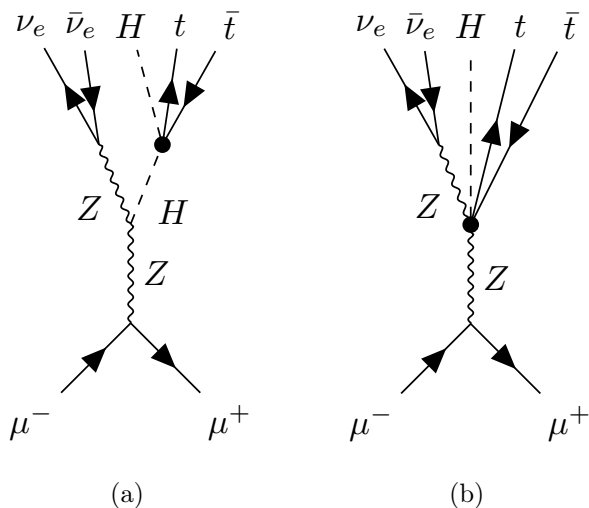


FIG. 8: Feynman diagram with the contact  $ttHH$  vertex (a) in both gauges and the that with  $ttHZZ$  vertex in the FD gauge (b).

first study the contribution of the diagram Fig.8(b), whose amplitude can be denoted as  $\mathcal{M}_{ttHZZ}$ . We find that

$$\mathcal{M}_{ttHZZ} = 0, \quad (23)$$

for all helicities at all energies. We attribute the cause of the vanishing amplitudes as a consequence of the fact that the virtual  $Z$  boson produced from massless lepton pair is purely transverse, and have no longitudinally polarized component. As a support of this observation, we find that all the amplitudes with higher dimensional operators whose Goldstone boson leg is connected directly to the initial state lepton pair are zero. In Table I, we have in total 62 diagrams contributing to the process (16), among which 16 diagrams have higher dimensional vertices, 1 at dimension-6, that of Fig.8(b), and the remaining 15 diagrams with dimension-5 vertices. There are 3 types of dimension-5 vertices,  $ttHH$  in Fig.8(a),  $ttHZ$ , and  $ttZZ$ . Feynman diagrams with  $ttHZ$  and  $ttZZ$  vertices where the vertex is connected by the FD gauge propagator directly to the initial  $\mu^- \mu^+$  current give zero amplitudes. The remaining 10 diagrams with dimension-5 vertices give non-zero amplitudes, 1 with  $ttHH$ , 8 with  $ttHZ$ , and 1 with  $ttZZ$  vertices. Since all these amplitudes with one dimension-5 vertex are expected to obey the same energy scaling law, we study the total sum of all the non-vanishing amplitudes with the dimension-5 vertices:

$$\left| \sum_k^{D5} \mathcal{M}_k \right|^2, \quad (24)$$

whose contribution is shown by the green dashed curve in Fig.7(b). As expected, the green dashed curve merges with the black solid curve at high energies,  $\sqrt{s} \gtrsim 50$  TeV. The total amplitudes in the FD gauge are dominated by the amplitudes with higher dimensional vertices as in the case of the amplitudes for the process (7) shown in Fig.4(b). The red curve remains slightly below the black and green curves, giving the ratio  $R \sim 0.83$  at  $\sqrt{s} \sim 100$  TeV in Fig.7(b). The constructive interference is observed among the 10 non-vanishing diagrams with dimension-5 vertices. This is in contrast to the case of the total cross section of the process (7) shown in Fig.4(b), where the ratio  $R \sim 1$  at high energies, reflecting the single diagram dominance.

## IV. SUMMARY

In this paper, we show how tree-level scattering amplitudes in the Feynman-Diagram (FD) gauge [2, 3] can be generated automatically in gauge models with non-Standard Model (SM) interactions.

- We start from the toolbox FEYNRULES [19], which can generate Feynman rules in the 't Hooft-Feynman gauge automatically for an arbitrary gauge model with spontaneous symmetry breaking.
- Based on the universal FEYNRULES output (UFO) [20, 21] in the Feynman gauge, we introduce 5-component representation of the weak bosons and their  $5 \times 5$  propagators automatically in MG5AMC [16].
- External 5-component weak boson polarization vectors and the  $5 \times 5$  weak boson propagators are common for all the gauge models, and we adopt the representations given in the original FD gauge papers [2, 3].
- Feynman diagrams for an arbitrary tree-level scattering amplitude with the 5-component weak bosons and their propagators can be generated on the flight by MG5AMC.
- All the vertex functions with and among 5-component weak bosons are obtained by assembling those of the 4-component weak bosons and the Goldstone bosons, which are generated automatically by using ALOHA [22] for an arbitrary gauge model.

The numerical codes for each Feynman diagram generated by the above procedure give helicity amplitudes in the FD gauge.

The above procedure has been explained in detail in section II. In section III, we demonstrate its validity by generating the helicity amplitudes for the muon collider process  $\mu^- \mu^+ \rightarrow \nu_\mu \bar{\nu}_\mu t \bar{t} H$  in an SMEFT [24–26] model with just one dimension-6 operator giving complex top Yukawa coupling [31]. 118 Feynman diagrams are generated in the FD gauge, as compared to the 89 diagrams in the unitary gauge. After summing over all the diagrams, we find exact agreement between the FD and the unitary gauges.

As in the case of the SM processes reported in refs. [1–3], the FD gauge amplitudes are free from subtle gauge cancellation among Feynman diagrams at high energies, thus

providing an efficient basis for numerical evaluation of the amplitudes. A new finding in this paper is that in the FD gauge, the high energy behavior of individual Feynman amplitude is dictated by the mass dimension of the contributing new physics vertex. In the weak boson fusion (WWF) amplitudes, the single diagram with a dimension-6  $ttHWW$  vertex dominates the total cross section at extreme high energies  $\sqrt{s} \sim 100$  TeV. Among the  $\mu^- \mu^+$  annihilation amplitudes, the corresponding amplitude with a dimension-6  $ttHZZ$  vertex is found to vanish, and the 10 non-vanishing amplitudes with a dimension-5 vertex ( $ttHH$ ,  $ttHZ$ ,  $ttZZ$ ) jointly dictate the high energy amplitudes at  $\sqrt{s} \gtrsim 50$  TeV.

The above example tells that the FD gauge amplitudes are useful in identifying the subamplitudes with non-SM interactions, because individual Feynman amplitude satisfies the naive scaling law;  $n$ -point amplitudes scale as  $E^{n-4}$  when all the vertices have mass dimension 4. The amplitude scales like  $E^{n-3}$  with one dimension-5 vertex, or  $E^{n-2}$  with one dimension-6 vertex, in the example studied in section III. This is an additional merit of the FD gauge, because the scaling law of the tree-level amplitudes is not manifest in covariant gauges, including the unitary gauge.

### Acknowledgement

We are grateful to Vernon Barger for enlightening discussions. This work is supported in part by JSPS KAKENHI Grant No. 21H01077 and 23K03403. KH is supported by the US Japan Cooperation Program in High Energy Physics.

- 
- [1] K. Hagiwara, J. Kanzaki, and K. Mawatari, “QED and QCD helicity amplitudes in parton-shower gauge,” *Eur. Phys. J. C* **80** (2020) no. 6, 584, [arXiv:2003.03003 \[hep-ph\]](#).
  - [2] J. Chen, K. Hagiwara, J. Kanzaki, and K. Mawatari, “Helicity amplitudes without gauge cancellation for electroweak processes,” *Eur. Phys. J. C* **83** (2023) no. 10, 922, [arXiv:2203.10440 \[hep-ph\]](#). [Erratum: *Eur.Phys.J.C* 84, 97 (2024)].
  - [3] J. Chen, K. Hagiwara, J. Kanzaki, K. Mawatari, and Y.-J. Zheng, “Helicity amplitudes in light-cone and Feynman-diagram gauges,” *Eur. Phys. J. Plus* **139** (2024) no. 4, 332, [arXiv:2211.14562 \[hep-ph\]](#).

- [4] K. Hagiwara, Q. Li, and K. Mawatari, “Jet angular correlation in vector-boson fusion processes at hadron colliders,” *JHEP* **07** (2009) 101, [arXiv:0905.4314 \[hep-ph\]](#).
- [5] A. Wulzer, “An Equivalent Gauge and the Equivalence Theorem,” *Nucl. Phys. B* **885** (2014) 97–126, [arXiv:1309.6055 \[hep-ph\]](#).
- [6] J. Chen, T. Han, and B. Tweedie, “Electroweak Splitting Functions and High Energy Showering,” *JHEP* **11** (2017) 093, [arXiv:1611.00788 \[hep-ph\]](#).
- [7] Z. Nagy and D. E. Soper, “Parton showers with quantum interference,” *JHEP* **09** (2007) 114, [arXiv:0706.0017 \[hep-ph\]](#).
- [8] Z. Nagy and D. E. Soper, “A parton shower based on factorization of the quantum density matrix,” *JHEP* **06** (2014) 097, [arXiv:1401.6364 \[hep-ph\]](#).
- [9] K. Hagiwara, H. Iwasaki, A. Miyamoto, H. Murayama, and D. Zeppenfeld, “Single weak boson production at TeV  $e^+ e^-$  colliders,” *Nucl. Phys. B* **365** (1991) 544–596.
- [10] R. Ruiz, A. Costantini, F. Maltoni, and O. Mattelaer, “The Effective Vector Boson Approximation in high-energy muon collisions,” *JHEP* **06** (2022) 114, [arXiv:2111.02442 \[hep-ph\]](#).
- [11] K. Hagiwara, H. Murayama, and I. Watanabe, “Search for the Yukawa interaction in the process  $e^+ e^- \rightarrow t \text{ anti-}t Z$  at TeV linear colliders,” *Nucl. Phys. B* **367** (1991) 257–286.
- [12] H. Murayama, I. Watanabe, and K. Hagiwara, “HELAS: HELicity amplitude subroutines for Feynman diagram evaluations,”.
- [13] T. Stelzer and W. F. Long, “Automatic generation of tree level helicity amplitudes,” *Comput. Phys. Commun.* **81** (1994) 357–371, [arXiv:hep-ph/9401258](#).
- [14] J. Alwall, P. Demin, S. de Visscher, R. Frederix, M. Herquet, F. Maltoni, T. Plehn, D. L. Rainwater, and T. Stelzer, “MadGraph/MadEvent v4: The New Web Generation,” *JHEP* **09** (2007) 028, [arXiv:0706.2334 \[hep-ph\]](#).
- [15] J. Alwall, M. Herquet, F. Maltoni, O. Mattelaer, and T. Stelzer, “MadGraph 5 : Going Beyond,” *JHEP* **06** (2011) 128, [arXiv:1106.0522 \[hep-ph\]](#).
- [16] J. Alwall, R. Frederix, S. Frixione, V. Hirschi, F. Maltoni, O. Mattelaer, H. S. Shao, T. Stelzer, P. Torrielli, and M. Zaro, “The automated computation of tree-level and next-to-leading order differential cross sections, and their matching to parton shower simulations,” *JHEP* **07** (2014) 079, [arXiv:1405.0301 \[hep-ph\]](#).
- [17] C. Becchi, A. Rouet, and R. Stora, “Renormalization of Gauge Theories,” *Annals Phys.* **98**

- (1976) 287–321.
- [18] I. V. Tyutin, “Gauge Invariance in Field Theory and Statistical Physics in Operator Formalism,” [arXiv:0812.0580 \[hep-th\]](#).
  - [19] A. Alloul, N. D. Christensen, C. Degrande, C. Duhr, and B. Fuks, “FeynRules 2.0 - A complete toolbox for tree-level phenomenology,” *Comput. Phys. Commun.* **185** (2014) 2250–2300, [arXiv:1310.1921 \[hep-ph\]](#).
  - [20] C. Degrande, C. Duhr, B. Fuks, D. Grellscheid, O. Mattelaer, and T. Reiter, “UFO - The Universal FeynRules Output,” *Comput. Phys. Commun.* **183** (2012) 1201–1214, [arXiv:1108.2040 \[hep-ph\]](#).
  - [21] L. Darmé *et al.*, “UFO 2.0: the ‘Universal Feynman Output’ format,” *Eur. Phys. J. C* **83** (2023) no. 7, 631, [arXiv:2304.09883 \[hep-ph\]](#).
  - [22] P. de Aquino, W. Link, F. Maltoni, O. Mattelaer, and T. Stelzer, “ALOHA: Automatic Libraries Of Helicity Amplitudes for Feynman Diagram Computations,” *Comput. Phys. Commun.* **183** (2012) 2254–2263, [arXiv:1108.2041 \[hep-ph\]](#).
  - [23] K. Fujikawa, B. W. Lee, and A. I. Sanda, “Generalized Renormalizable Gauge Formulation of Spontaneously Broken Gauge Theories,” *Phys. Rev. D* **6** (1972) 2923–2943.
  - [24] C. N. Leung, S. T. Love, and S. Rao, “Low-Energy Manifestations of a New Interaction Scale: Operator Analysis,” *Z. Phys. C* **31** (1986) 433.
  - [25] W. Buchmuller and D. Wyler, “Effective Lagrangian Analysis of New Interactions and Flavor Conservation,” *Nucl. Phys. B* **268** (1986) 621–653.
  - [26] B. Grzadkowski, M. Iskrzynski, M. Misiak, and J. Rosiek, “Dimension-Six Terms in the Standard Model Lagrangian,” *JHEP* **10** (2010) 085, [arXiv:1008.4884 \[hep-ph\]](#).
  - [27] X. Zhang, S. K. Lee, K. Whisnant, and B. L. Young, “Phenomenology of a nonstandard top quark Yukawa coupling,” *Phys. Rev. D* **50** (1994) 7042–7047, [arXiv:hep-ph/9407259](#).
  - [28] K. Whisnant, B.-L. Young, and X. Zhang, “Unitarity and anomalous top quark Yukawa couplings,” *Phys. Rev. D* **52** (1995) 3115–3118, [arXiv:hep-ph/9410369](#).
  - [29] M. Chen and D. Liu, “Top Yukawa coupling measurement at the muon collider,” *Phys. Rev. D* **109** (2024) no. 7, 075020, [arXiv:2212.11067 \[hep-ph\]](#).
  - [30] Z. Liu, K.-F. Lyu, I. Mahbub, and L.-T. Wang, “Top Yukawa coupling determination at high energy muon collider,” *Phys. Rev. D* **109** (2024) no. 3, 035021, [arXiv:2308.06323 \[hep-ph\]](#).
  - [31] V. Barger, K. Hagiwara, and Y.-J. Zheng, “CP-violating top-Higgs coupling in SMEFT,”

- Phys. Lett. B* **850** (2024) 138547, [arXiv:2310.10852 \[hep-ph\]](#).
- [32] M. E. Cassidy, Z. Dong, K. Kong, I. M. Lewis, Y. Zhang, and Y.-J. Zheng, “Probing the CP Structure of the Top Quark Yukawa at the Future Muon Collider,” [arXiv:2311.07645 \[hep-ph\]](#).
- [33] Z. Kunszt and D. E. Soper, “On the Validity of the Effective  $W$  Approximation,” *Nucl. Phys. B* **296** (1988) 253–289.
- [34] S. Dawson, “The Effective  $W$  Approximation,” *Nucl. Phys. B* **249** (1985) 42–60.
- [35] J. M. Cornwall, D. N. Levin, and G. Tiktopoulos, “Derivation of Gauge Invariance from High-Energy Unitarity Bounds on the  $s$  Matrix,” *Phys. Rev. D* **10** (1974) 1145. [Erratum: *Phys.Rev.D* **11**, 972 (1975)].
- [36] M. S. Chanowitz and M. K. Gaillard, “The TeV Physics of Strongly Interacting  $W$ ’s and  $Z$ ’s,” *Nucl. Phys. B* **261** (1985) 379–431.
- [37] J. F. Gunion, B. Grzadkowski, and X.-G. He, “Determining the top - anti-top and  $Z Z$  couplings of a neutral Higgs boson of arbitrary CP nature at the NLC,” *Phys. Rev. Lett.* **77** (1996) 5172–5175, [arXiv:hep-ph/9605326](#).
- [38] P. S. Bhupal Dev, A. Djouadi, R. M. Godbole, M. M. Muhlleitner, and S. D. Rindani, “Determining the CP properties of the Higgs boson,” *Phys. Rev. Lett.* **100** (2008) 051801, [arXiv:0707.2878 \[hep-ph\]](#).
- [39] B. Ananthanarayan, S. K. Garg, C. S. Kim, J. Lahiri, and P. Poulose, “Top Yukawa coupling measurement with indefinite CP Higgs in  $e^+e^- \rightarrow t\bar{t}\Phi$ ,” *Phys. Rev. D* **90** (2014) no. 1, 014016, [arXiv:1405.6465 \[hep-ph\]](#).
- [40] K. Hagiwara, H. Yokoya, and Y.-J. Zheng, “Probing the CP properties of top Yukawa coupling at an  $e^+e^-$  collider,” *JHEP* **02** (2018) 180, [arXiv:1712.09953 \[hep-ph\]](#).
- [41] K. Ma, “Enhancing  $CP$  Measurement of the Yukawa Interactions of Top-Quark at  $e^-e^+$  Collider,” *Phys. Lett. B* **797** (2019) 134928, [arXiv:1809.07127 \[hep-ph\]](#).
- [42] D. Azevedo, R. Capucha, A. Onofre, and R. Santos, “CP-violation, asymmetries and interferences in  $t\bar{t}\phi$ ,” *JHEP* **09** (2022) 246, [arXiv:2208.04271 \[hep-ph\]](#).
- [43] K. Cheung, Y.-n. Mao, S. Moretti, and R. Zhang, “Testing CP-violation in a Heavy Higgs Sector at CLIC,” [arXiv:2304.04390 \[hep-ph\]](#).